Dynamics of short-pulse splitting in dispersive nonlinear media

Marek Trippenbach and Y. B. Band
Departments of Chemistry and Physics, Ben-Gurion University of the Negev, Beer-Sheva 84105, Israel
(Received 9 January 1997; revised manuscript received 17 June 1997)

We develop a method to precisely propagate short optical pulses through dispersive media with a cubic self-focusing nonlinear polarization. We show that above the critical cw self-focusing power, onset of pulse splitting into pulselets separated in time occurs, and for a certain regime of parameters a *cyclic series* of pulse splitting (into pulselets separated in time) and pulse recombination occurs for diffraction length smaller than dispersion length. At higher power, *another* threshold for noncyclic temporal and spatial pulse splitting is manifest. The physics of these phenomena are described and delineated. [S1050-2947(97)07211-9]

PACS number(s): 42.65.Re, 42.25.Fx, 42.65.Sf

I. INTRODUCTION

Nonlinear dispersive systems are omnipresent in nature. One such system that has been of great interest and importance since the advent of intense short-pulse light sources is that of temporally short optical pulses propagating in isotropic dispersive nonlinear media. This system has a plethora of technological and scientific applications. Many recent studies [1–7] have shown that pulse splitting occurs in $\chi^{(3)}$ media for pulses with powers beyond the threshold for self-focusing (SF). Here we show that the phenomena associated with pulse splitting of intense short optical pulses are considerably more complicated and elaborate than previously imagined. Specifically, we find that in the normal dispersion regime, above the threshold for SF, there are two separate mechanisms for pulse splitting, the second mechanism occurring only for pulse intensities above a high intensity threshold. The lower threshold is for temporal pulse splitting (for diffraction length smaller than dispersion length), wherein the pulse splits apart in time. For a certain regime of parameters (to be specified below), a cyclic series of pulse splitting and pulse recombination into pulselets separated in time occurs. Thus pulses carry out a series of (a) splitting into two pulselets separated in time, and (b) recombination into a central peak; this dance of splitting and recombining cyclicly recurs. In the Fourier (frequency and wave-vector) domain, an annular ring forms around the central peak, then the ring splits apart into separate peaks. For pulse intensities above the higher threshold, temporal and spatial pulse splitting occurs (but the cyclic process does not occur). This is a new mechanism for pulse splitting corresponding to splitting of pulses in both time and transverse space dimensions; it occurs for intensities above the higher threshold, with multiple pulse breakup transpiring as the pulse propagates. We demonstrate these phenomena using an exact numerical method to propagate short pulses in a nonlinear dispersive medium, with dispersion and diffraction treated to all order, as is necessary for a quantitative description, but the phenomena occur even when a second-order expansion of the nonlinear Schrödinger equation is used. We also present results for the anomalous dispersion regime and the regime where the group velocity dispersion vanishes. Pulse splitting occurs in these regimes, but the details of the splitting phenomena are different than in the normal dispersion regime. We also investigate the effects of self-steepening on these phenomena.

Section II describes the propagation equations used to carry out the pulse dynamics, Sec. III contains the numerical results, and Sec. IV contains a summary and conclusion. The Appendix contains details regarding the derivation of the wave equation used to propagate pulses.

II. PROPAGATION EQUATION

The propagation equation for the slowly varying envelope of the electric field (SVE), $\vec{A}(\vec{x},t)$, can be derived by differentiating it with respect to the position coordinate in the direction of the central wave vector $\vec{K}_0$, $\vec{s}_0=\vec{K}_0/|K_0|$, which we choose to be along the space-fixed z axis [8–10]. For linearly polarized light

$$\frac{\partial\vec{A}(\vec{x},t)}{\partial z}=\frac{1}{(2\pi)^4}\int_{-\infty}^{+\infty}d^3Kd\omega\vec{A}(\vec{K},\omega)(i[\vec{K}-\vec{K}_0]\cdot\vec{s}_0)\times e^{i([\vec{K}-\vec{K}_0]\cdot\vec{x}-[\omega-\omega_0]t)}+i\gamma_{\rm nl}|\vec{A}|^2\vec{A}, \quad (1)$$

where $\gamma_{\rm nl}=2\pi\chi^{(3)}\omega_0/[n(\omega_0)c]$. The details of the derivation are presented in the Appendix.

Due to the dispersion relation, the variables $\vec{K}$ and ω are not independent and the four dimensional integrals in the first term on the right hand side of Eq. (1) can be reduced to three dimensions. For numerical applications we eliminate the integral over K_z, using the dispersion relation to express K_z in terms of K_x, K_y, and ω: $K_z=\sqrt{\omega^2n(\omega)^2/c^2-K_x^2-K_y^2}$. A partial differential equation (PDE) for the SVE can be obtained by using this expression, expanding K_z appearing in Eq. (1) in powers of K_x, K_y, and $(\omega-\omega_0)$ and replacing these variables with $i\partial/\partial x$, $i\partial/\partial y$, and $-i\partial/\partial t$, respectively [8]. In what follows we consider a linearly polarized incident field in an isotropic medium and therefore we focus on one component of the SVE. Keeping terms up to third order, the PDE for A is [8]

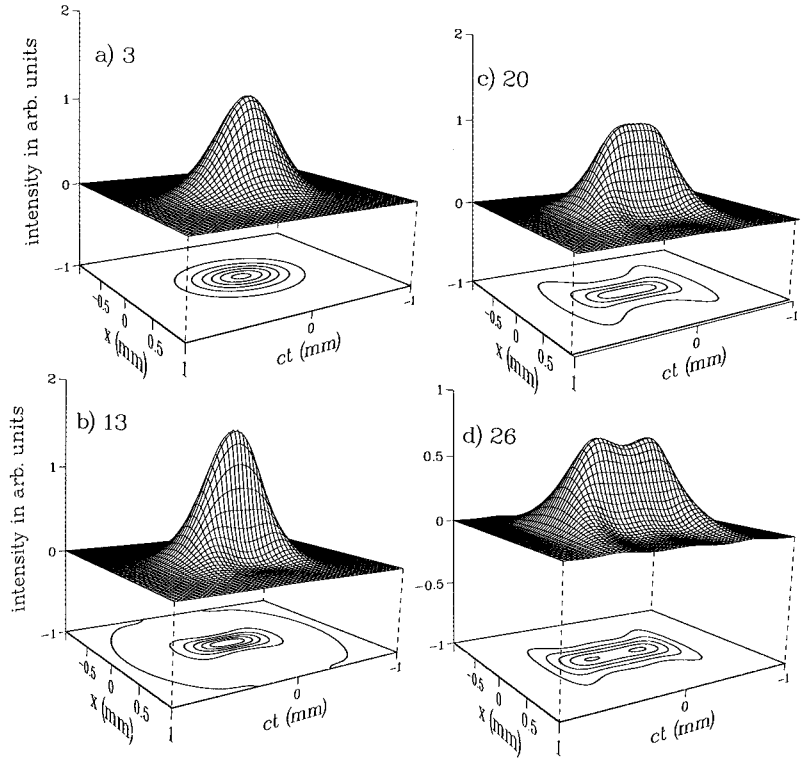

FIG. 1. Pulse intensity versus x and ct for various propagation distances L_z (in mm) as indicated next to the label, for wide pulse and lower intensity.

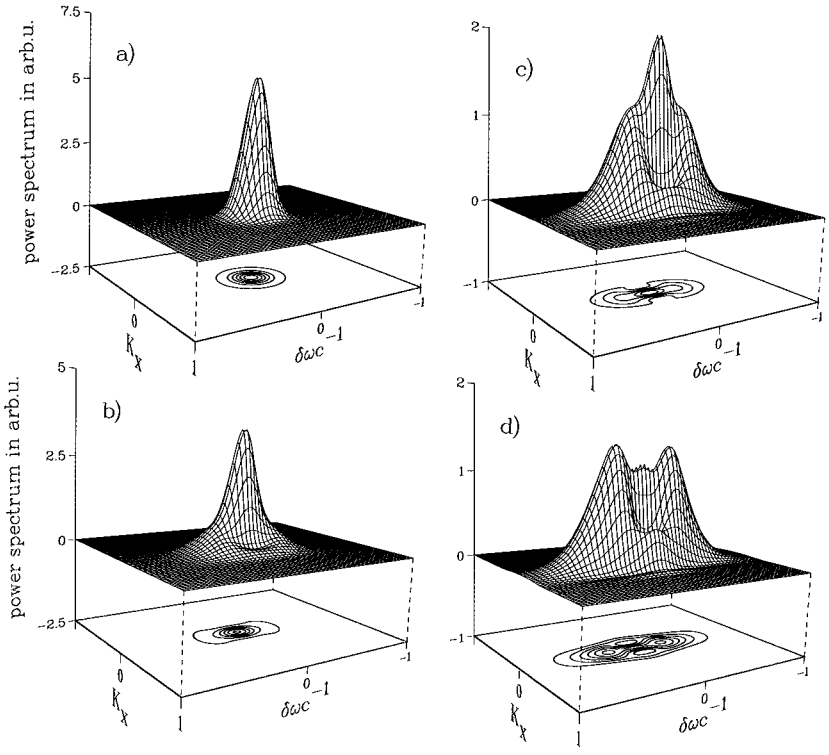

FIG. 2. Power spectrum versus $\delta\omega/c=(\omega-\omega_0)/c$ and K_x corresponding to Fig. 1.

$$\frac{\partial A}{\partial z} = -\beta_1 \frac{\partial A}{\partial t} - \frac{i}{2}\beta_2 \frac{\partial^2 A}{\partial t^2} + \frac{1}{6}\beta_3 \frac{\partial^3 A}{\partial t^3} + \frac{i}{2}\gamma_{xx} \times \left(\frac{\partial^2 A}{\partial x^2} + \frac{\partial^2 A}{\partial y^2}\right) d + \frac{1}{3}\gamma_{txx}\left(\frac{\partial^3 A}{\partial x^2 \partial t} + \frac{\partial^3 A}{\partial y^2 \partial t}\right) + i\gamma_{\mathrm{nl}}|A|^2 A, \tag{2}$$

where β_1 is the inverse group velocity, β_2 the group velocity dispersion, β_3 the third-order dispersion, γ_{xx} the Fresnel diffraction coefficient, and γ_{txx} the coefficient of the mixed space-time third-order terms that account for the spherical nature of the wave front surface of a pulse originating from a point source. For a cylindrically symmetric pulse of width w_0, or for a pulse whose transverse y dimension is large and can therefore be ignored, Eq. (2) can be written in terms of the following lengths (the smaller the length, the more important the corresponding term in the PDE): diffraction length $L_{\mathrm{df}} = \gamma_{xx} w_0^2/2 = \pi w_0^2/\lambda_0$, dispersion length $L_{\mathrm{ds}} = \tau_0^2/\beta_2$, third-order dispersion length $L_{\mathrm{TOD}} = \tau_0^3/\beta_3$, third-order dispersion-diffraction length, $L_{\mathrm{dsdf}} = \tau_0 w_0^2/\gamma_{txx}$, and nonlinear length $L_{\mathrm{nl}} = (\gamma_{\mathrm{nl}}|A_0|^2)^{-1}$ where A_0 is the peak amplitude of the pulse. Since $\gamma_{xx} = c/[n(\omega_0)\omega_0]$, L_{df} is positive in all our studies. The propagation equation can be written explicitly in terms of these length scales as follows:

$$\frac{\partial A}{\partial z} = -\beta_1 \frac{\partial A}{\partial t} - i\frac{\tau_0^2}{L_{\mathrm{ds}}}\frac{\partial^2 A}{\partial t^2} + \frac{\tau_0^3}{L_{\mathrm{TOD}}}\frac{\partial^3 A}{\partial t^3} + i\frac{w_0^2}{L_{\mathrm{df}}}\left(\frac{\partial^2 A}{\partial x^2} + \frac{\partial^2 A}{\partial y^2}\right) + \frac{w_0^2 \tau_0}{L_{\mathrm{dsdf}}}\left(\frac{\partial^3 A}{\partial x^2 \partial t} + \frac{\partial^3 A}{\partial y^2 \partial t}\right) + i\frac{1}{|A_0|^2 L_{\mathrm{nl}}}|A|^2 A. \tag{3}$$

When the propagation equation is written in this form, it is easy to determine the relative importance of each of the terms in the equation based upon the size of the corresponding length scales. Moreover, the length scale indicates at what value of propagation distance L_z the corresponding phenomenon is expected to become significant. Furthermore, if we go to a frame moving with the pulse (by making a transformation of the form $z \Rightarrow z - t/\beta_1$) we eliminate the β_1 term from the propagation equation.

The following scaling property of the propagation equation is worthy of note. If we restrict the expansion to second order in Eq. (3), and scale w_0, τ_0, A_0, and L_z to ζw_0, $\zeta \tau_0$, A_0/ζ, and $\zeta^2 L_z$, respectively, then the ratios of the lengths $L_{\mathrm{ds}}:L_{\mathrm{df}}:L_{\mathrm{nl}}:L_z$ remain unchanged. Therefore the second-order pulse propagation dynamics in terms of the scaled variables is exactly as in the unscaled second-order dynamics.

The nonlinear length corresponding to critical cw self-focusing $L_{\mathrm{nl,CSF}}$ is given in the literature [2] as $L_{\mathrm{nl,CSF}} = 1.887 L_{\mathrm{df}}$. Two conditions must be met for self-focusing to occur: (1) the pulse power P must exceed the medium's critical power, $P_{\mathrm{cr}} = (0.61)^2 \lambda_0^2 n_0 c/(32\pi\chi^{(3)})$, and (2) the fluence must remain smaller than the medium's damage threshold fluence F_{dmg} (in units of, say, J/cm^2) [12]. For a pulse of initial spot size w_0^2 and initial temporal duration τ_0, the power corresponding to the damage fluence F_{dmg} is $P_{\mathrm{dmg}} = F_{\mathrm{dmg}} w_0^2/\tau_0$. As long as $P_{\mathrm{cr}} < P < P_{\mathrm{dmg}}$, SF can proceed without damaging the medium.

The above damage threshold considerations restrict the applications of scaling of the second-order expansion of Eq. (3) as follows: Threshold power for SF does not depend on the pulse cross section. The power corresponding to the damage threshold, however, depends on pulse duration and cross

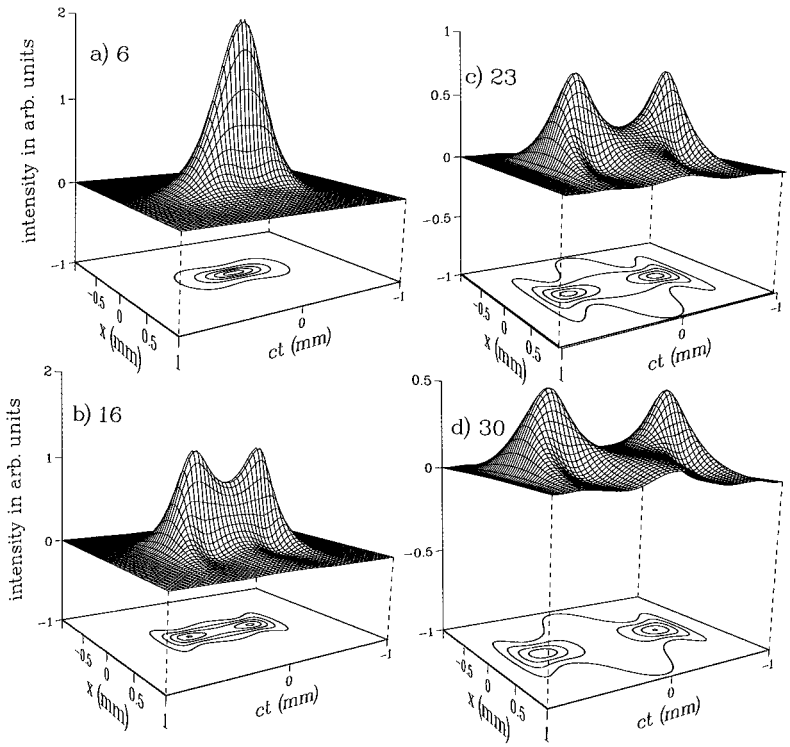

FIG. 3. Pulse intensity versus x and ct for various propagation distances L_z (in mm) for wide pulse and medium intensity.

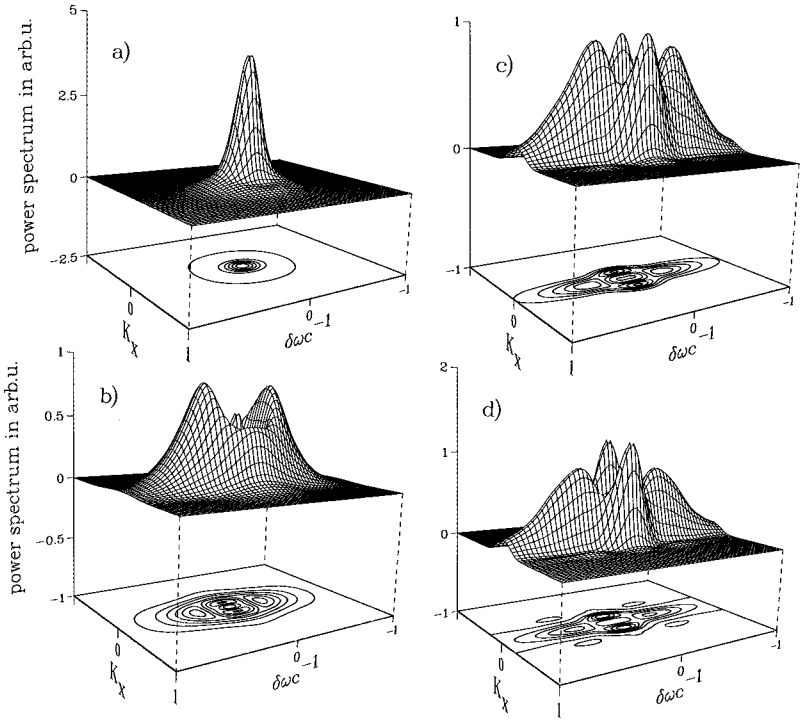

FIG. 4. Power spectrum versus $\delta\omega/c$ and K_x corresponding to Fig. 3.

section. The range of intensities available for nondamaging SF decreases as the pulse width and temporal duration decrease.

III. NUMERICAL RESULTS

In all numerical results presented here, Eq. (1) was used, but the third-order expansion, Eq. (2) or (3), yields results close to the exact ones. For presentation purposes, we take the y transverse width to be very large and plot the propagation results vs x and ct for various propagation distances L_z [11]. In what follows we consider pulse propagation in silica (SiO_2). We choose the following pulse parameters: in the normal dispersion regime we take the central wavelength $\lambda_0=800$ nm, temporal pulse duration $\tau_0=66$ fs, and initial spot size of $w_0=12\lambda_0$ and $40\lambda_0$ for the small and large spot size case, respectively. For $w_0=12\lambda_0(\approx 10\ \mu\text{m})$, $L_{\text{df}}=362\mu<L_{\text{dsdf}}=7.7\times10^4\ \mu m<L_{\text{ds}}=2.4\times10^5\mu\text{m}\ll L_{\text{TOD}}=1.1\times10^7\ \mu\text{m}$. For $w_0=40\lambda_0$ ($32\ \mu\text{m}$), $L_{\text{df}}=4021\ \mu\text{m}<L_{\text{ds}}=2.4\times10^5\ \mu\text{m}<L_{\text{dsdf}}=8.5\times10^5\ \mu\text{m}\ll L_{\text{TOD}}=1.1\times10^7\ \mu\text{m}$. In the anomalous dispersion regime we shall take a wavelength of $\lambda_0=1400$ nm, and in the zero dispersion regime, the central wavelength is $\lambda_0=1270$ nm.

A. Normal dispersion regime

We consider first the normal dispersion regime ($\lambda_0=800$ nm). We begin by presenting results for the case of $w_0=40\lambda_0$ ($32\ \mu\text{m}$) since the dynamics is less complicated for this case of relatively large pulse width. We take a relatively low intensity of 4.7×10^{10} W/cm^2, which corresponds to a power just above the SF threshold ($P/P_{\text{cr}}=1.5$) corresponding to a nonlinear length, $L_{\text{nl}}=5000\ \mu\text{m}$. For this set of parameters, the shortest length scale is L_{df}, with L_{nl} about 20% larger. We shall plot three dimensional (3D) surfaces and contour plots of $|A(x,y,z,t)|^2$ versus ct and x for various propagation distances of L_z in the frame traveling with the group velocity [and the Fourier transforms $|A(K_xK_y,K_z,\omega)|^2$ versus $(\omega-\omega_0)/c$ and K_x]. Figure 1 shows the pulse propagation dynamics as a function of propagation distance L_z. Self-phase modulation (SPM) due to the nonlinear polarization is strongest at the center of the pulse (small t and x); this widens the spectral distribution, and group velocity dispersion (GVD) spatially separates the different colors in the pulse. Hence, the pulse splits into two pulselets, but diffraction effects are very strong and dominate the dynamics after the temporal pulse spitting occurs. Note that in Fig. 1 we have plotted only a small fraction of the x and ct space region over which the computation was performed (hence the actual boundary is much larger than the boundary shown in the figure). This is true of all of the figures (we have checked to make sure there is no reflection off the actual boundary). Figure 2 shows the Fourier transform picture of the results shown in Fig. 1. The dominant effect in Fig. 2 is the development of a bimodal distribution of frequencies around the central frequency. The lower (higher) frequency distribution travels faster (slower) in time and gives rise to the forward (backward) peak in Fig. 1.

Figures 3 and 4 are for a slightly higher intensity (7.0×10^{10} W/cm^2, corresponding to a power such that $P/P_{\text{cr}}=2.2$) but are otherwise similar to Figs. 1 and 2. Now, the formation of an annular ring in momentum space, which was barely perceptible for the lower intensity, is clearly seen. This ring structure evolves into a four peaked distribution having peaks at higher and lower frequency and two peaks at

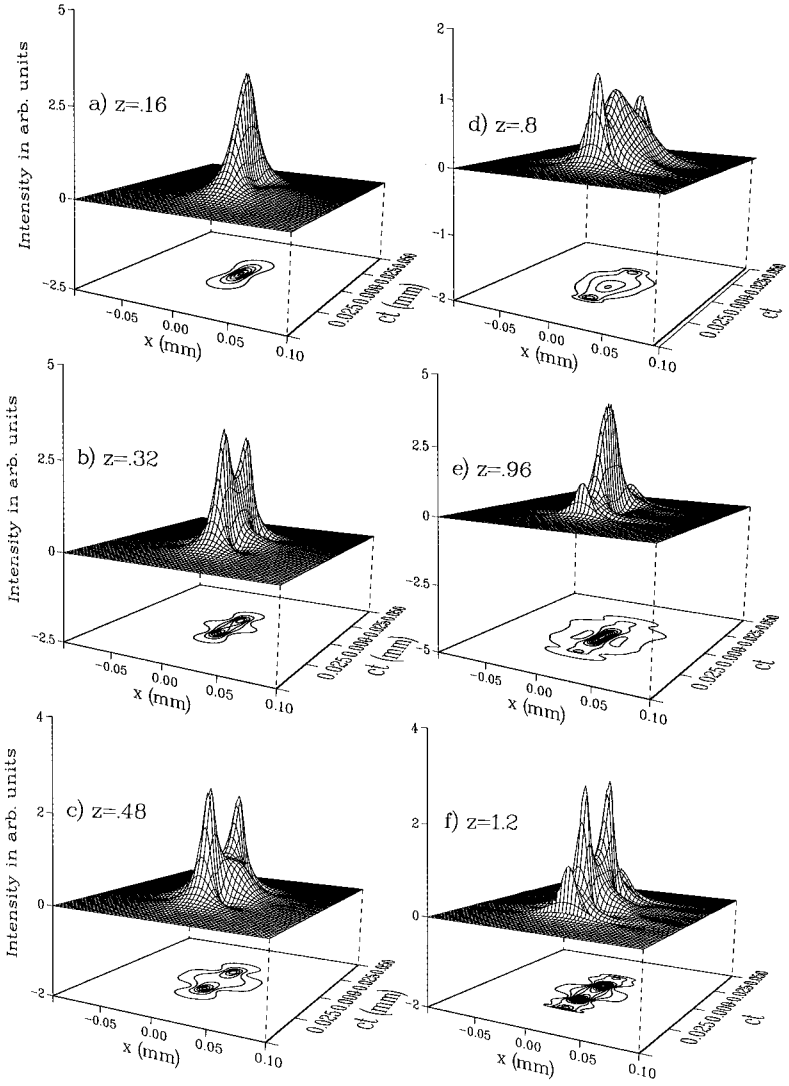

FIG. 5. Pulse intensity versus x and ct for various propagation distances L_z (in mm) for narrow pulse width.

the central frequency with high and low momenta. In position-time space, these momentum satellites are responsible for the wide shoulders at $t=0$.

We now present results for the smaller initial width, $w_0=12\lambda_0$. We keep the pulse duration unchanged, hence diffraction effects are enhanced over dispersion since $L_{\rm df}/L_{\rm ds}$ is decreased. With the damage related restrictions mentioned above in mind, we choose a sufficiently low intensity to avoid damage; we take $I=2\times10^{12}$ W/cm^2. The progression in the pulse propagation dynamics with increasing L_z is as follows when $L_{\rm nl}\approx L_{\rm df}<L_{\rm ds}$: (a) The nonlinearity causes SF of the pulse [see reduced transverse dimension in Fig. 5(a)]. The focusing is strongest near the peak of the pulse around $t=0$. In ω-K_x space, the power spectrum develops an annular ring around the central peak. (b) SF is strongest near $t=0$ and pulls the pulse into small x most strongly near $t=0$. At medium range values of x, a hole develops near $t=0$ [see contour lines on the 3D plot of Fig. 5(a)]. (c) SPM due to the nonlinearity is strongest at the center of the pulse (small t and x); this widens the spectral distribution. In ω-K_x space, the intensity of the annular ring increases at large ω and decreases at large K_x thereby deforming the ring, and eventually turning it into a two-bulged structure centered at $\omega_0\pm\Omega$ where Ω grows with increasing z due to GVD [see Fig. 4(d)]; this spectral widening of the pulse occurs despite $L_{\rm ds}\ll L_z$, since SPM introduces significant additional bandwidth. (d) Temporal pulse splitting occurs as SF continues to pull the pulse into small x, the hole at medium x and small t is pulled into small x, and GVD disperses the intensity away from $t=0$ [see Figs. 5(b) and 5(c)]. (e) The γ_{xxt} term causes asymmetry between the leading and trailing pulselets [1] with the trailing peak being more intense [Figs. 5(b)–5(d)]; in the normal dispersion regime the leading (trailing) pulselets are redshifted (blueshifted). (f) As the hole at small t and x becomes pronounced, the intensity in this region falls and the SF cannot prevent the dispersion from pushing the intensity which had been self-focused at small x outward in x [Figs. 5(c) and 5(d)]. Pulse widens in x at small t but remains adjoined (as we shall see this is not a case at higher intensities, above the spatial pulse splitting threshold). (g) Intensity at small x and small t is filled in and a central high intensity peak is formed at the expense of the leading and trailing pulselets [Figs. 5(d) and 5(e)]. The processes seen in Figs.

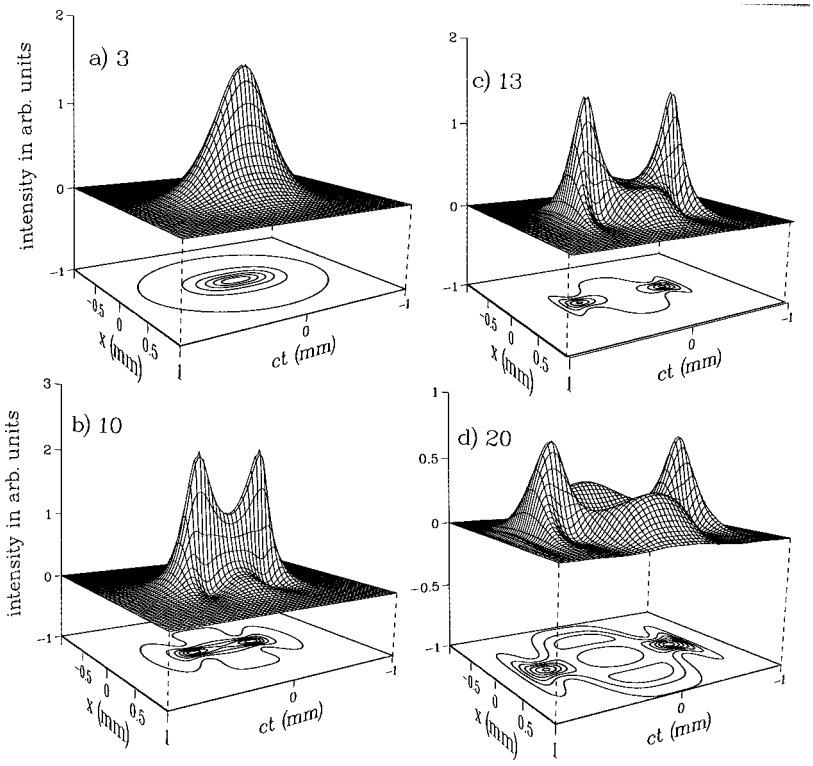

FIG. 6. Pulse intensity versus x and ct for various propagation distances L_z (in mm) for wide pulse and high intensity.

5(a)–5(e) begin over again [see Fig. 5(f), which is similar to Fig. 5(b)] and the process cyclicly recurs a few times.

The next example illustrates the dynamics of spatial pulse splitting. We have chosen an initial pulse of spot size $w_0 = 40\lambda_0$, but a higher intensity of 1.1×10^{11} W/cm^2. SF initially leads to temporal pulse splitting, but this is followed by formation of two additional satellite peaks centered at $t=0$ and nonzero x, as shown in Fig. 6. If the pulse intensity is high enough, satellite peaks may undergo futher temporal splitting, before dispersion and diffraction smear out the structure. This splitting of the side peaks leads to the multi-peak structure observed in the autocorrelation measurements

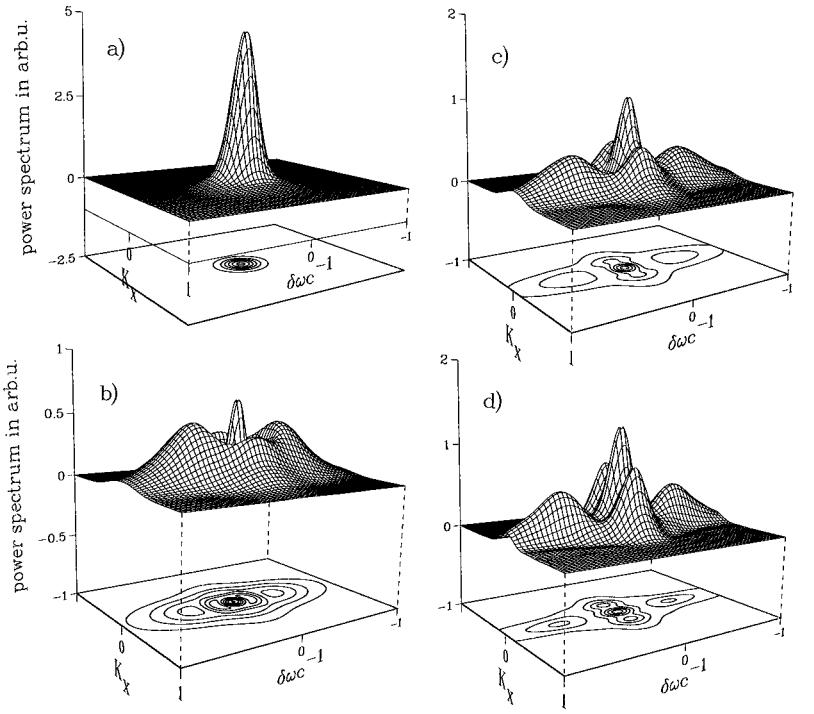

FIG. 7. Power spectrum versus $\delta\omega/c$ and K_x corresponding to Fig. 6.

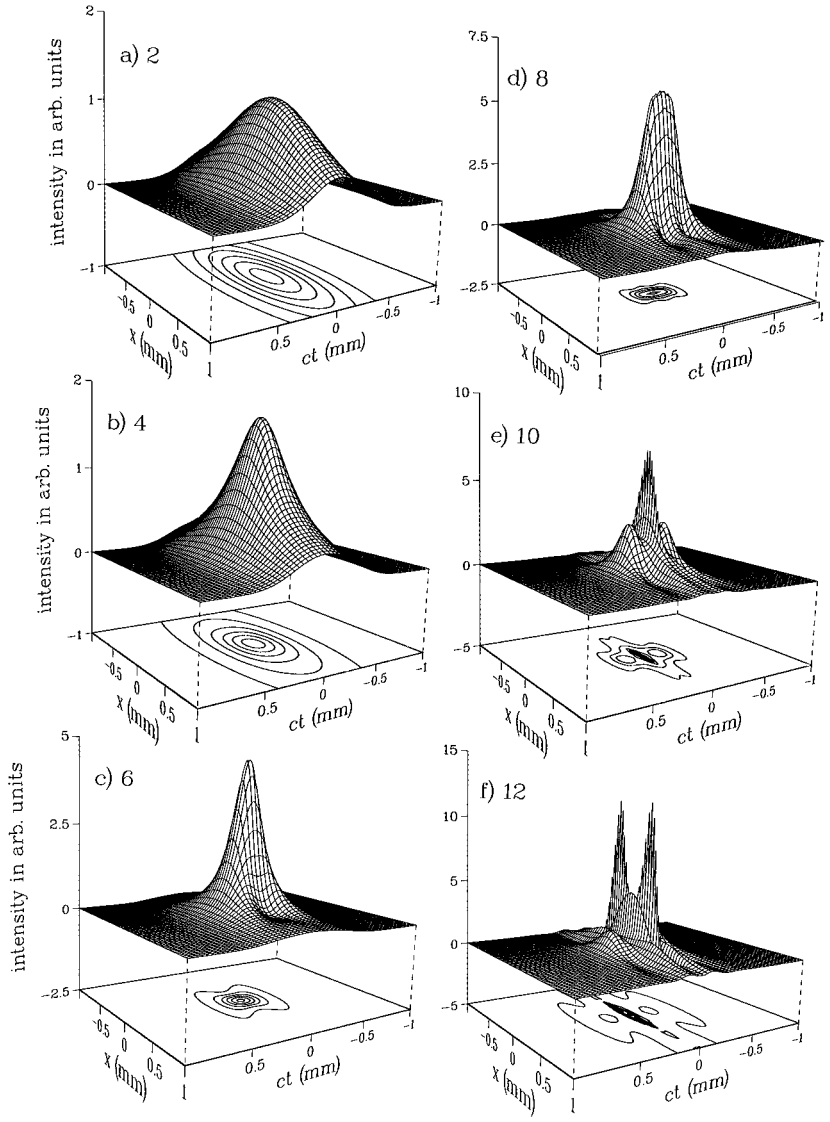

FIG. 8. Pulse intensity versus x and ct for various propagation distances L_z (in mm) in the anomalous dispersion regime.

[4]. In Fourier space, the intial peak transforms into a ''Mexican hat'' structure having an annular ring and then transforming into a structure containing two peaks at finite $\delta\omega$, two sideband peaks symmetric around $K_x=0$, and a central peak centered at $K_x=0$, $\delta\omega=0$, as shown in Fig. 7.

B. Anomalous dispersion regime

We now present results of our calculations in the anomalous dispersion regime $\lambda_0=1400$ nm. The temporal pulse duration is again taken to be $\tau_0=66$ fs, and the initial spot size is $40\lambda_0$ and intensity 6.0×10^{10} W/cm^2. The length scales of this case are $L_{\rm df}=703$ μm$<L_{\rm dsdf}=8.6\times10^4$ μm$<|L_{\rm ds}|=6.9\times10^5$ μm (but negative). Note that in the anomalous dispersion regime where $\beta_2<0$, a symmetry exists with respect to the t and the position coordinates x and y, in the sense that the signs of the corresponding coefficients in the propagation equation are identical in the anomalous dispersion regime. Figure 8 shows the pulse propagation dynamics as a function of propagation distance L_z. We again see the self-focusing of the pulse and eventually the pulse splits in time. The central peak in time is extremely short. This extremely short temporal duration peak ultimately splits apart in the transverse spatial dimension. Figure 9 shows the power spectrum. Amazingly, no splitting is evident in momentum space. What is present is a very wide pedestal in frequency which develops near $K_x=0$. If $L_{\rm df}>|L_{\rm ds}|$, the role of x and t would be largely reversed from that shown in Fig. 8 (but not completely since the effects of the γ_{txx} term are not completely negligible); the pulse would ''self-focus in time.'' Hence, in the anomalous regime above the self-focusing threshold, transverse spatial pulse splitting occurs first (rather than temporal pulse splitting) for diffraction length larger than the dispersion length (very wide pulses).

C. Zero dispersion regime

Figure 10 shows the pulse propagation dynamics for a pulse with the same parameters as in Figs. 8 and 9 but intensity 4.4×10^{10} W/cm^2 and central wavelength of $\lambda_0=1270$ nm, where $\beta_2=0$ (hence $L_{\rm ds}=0$). The pulse self-focuses and then splits into two pulselets but the leading pulse is much more intense than the trailing pulse. The self-focusing of the leading pulselet is more pronounced than that of the trailing pulselet. The Fourier transform picture in Fig. 11 shows the

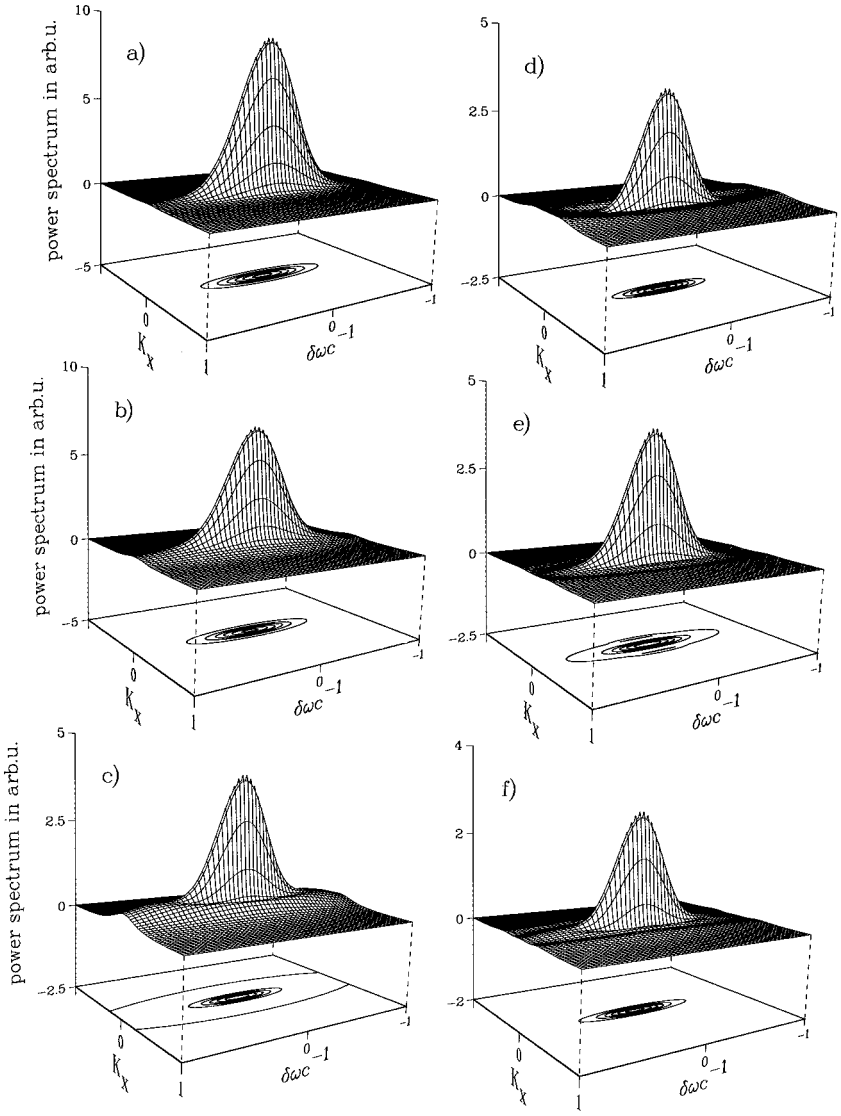

FIG. 9. Power spectrum versus $\delta\omega/c$ and K_x corresponding to Fig. 8.

initial formation of an annular ring which breaks up into pulselets in the normal and anomalous dispersion regimes. The pulselets on either side of the central frequency travel at different speeds, thereby accounting for the breakup of the central peak in position space. These pulselets are nonsymmetric in their intensity, the lower frequency having more power.

D. Self-steepening

In order to determine whether the nonlinear effects of self-steepening are important, we added a term to the right hand side of Eq. (2) of the form $\gamma_{\rm nl}\omega_0^{-1}\partial(|A|^2A)/\partial t$ (see Appendix and [13]). For all of the cases studied here, except one, no noticeable effects of self-steepening were observed over the propagation distances used. The exception is the case of anomalous dispersion, where the central (in time) pulselet became extremely short. The time derivative in the self-steepening nonlinear polarization term therefore becomes large, even for the initial pulse duration of 66 fs used in our simulation. A careful study of this effect will be presented elsewhere.

IV. SUMMARY AND CONCLUSION

In summary, we have described the propagation of short optical pulses in isotropic media for intensities above the self-focusing threshold in the normal, anomalous, and zero dispersion regimes. We have shown that above the critical cw self-focusing power, onset of pulse splitting into pulselets separated in time occurs for diffraction length smaller than dispersion length. For sufficiently long dispersion length, a cyclic series of pulse splitting (into pulselets separated in time) and pulse recombination occurs. At higher power, another threshold exists for noncyclic spatial pulse splitting for diffraction length smaller than dispersion length. Although pulse splitting occurs in normal, anomalous, and zero dispersion regimes, we saw that the details of the pulse splitting are different in these regimes. In particular, in the anomalous regime the pulse did not break apart in frequency-momentum space, only in physical space. This indicates that pulse chirp is more important to pulse splitting in this regime. In the zero dispersion regime we saw the asymmetry of the leading and trailing pulselets; their intensity and spatial and temporal widths are substantially different. In the range of parameters

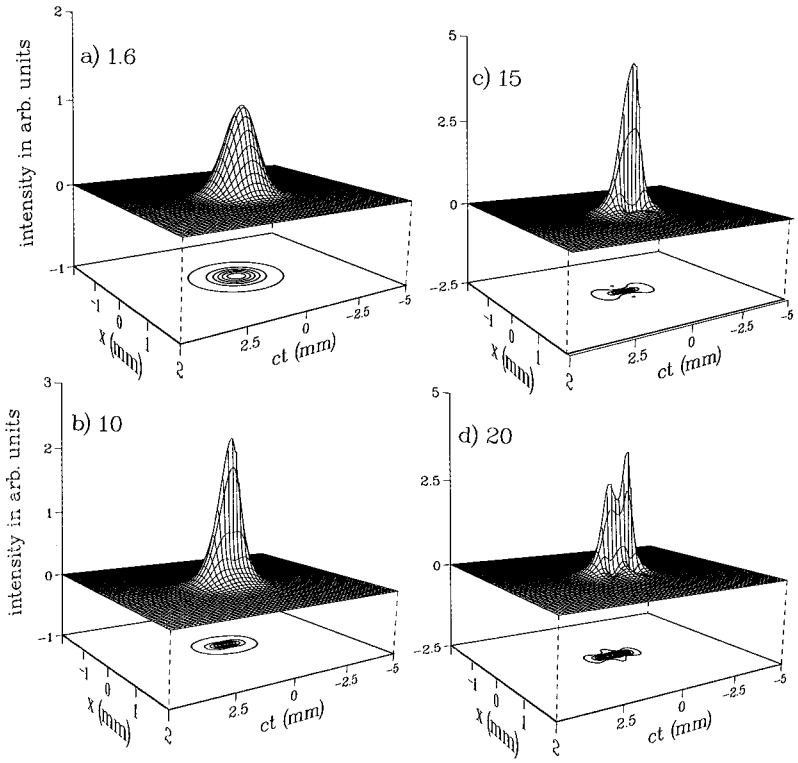

FIG. 10. Pulse intensity versus x and ct for various propagation distances L_z (in mm) in the zero dispersion regime.

studied here self-steepening does not affect the pulse propagation dynamics in all but the anomalous dispersion regime where part of the pulse becomes extremely narrow in time. It remains to investigate these phenomena in crystals where walkoff and pulse rotation play an important role [8–10].

ACKNOWLEDGMENTS

This work was supported in part by grants from the US-Israel Binational Science Foundation and the Israel Academy of Science. We thank Eduard Merzlyakov for assistance with graphics.

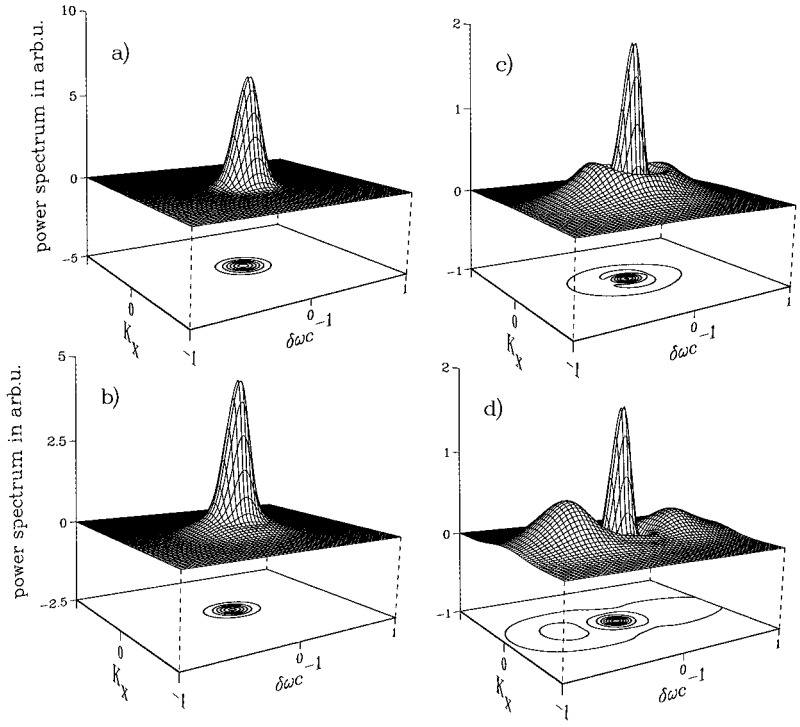

FIG. 11. Power spectrum versus $\delta\omega/c$ and K_x corresponding to Fig. 10.

APPENDIX

The purpose of this appendix is to describe the derivation of the nonlinear propagation wave equation for an isotropic dispersive medium. We begin by describing the dispersion relation, and then proceed to consider the linear and nonlinear optical susceptibilities.

1. Dispersion relation

We derive the nonlinear dispersion relation in an optically isotropic dispersive medium. We begin by writing down the Ampere and Faraday equations (in Gaussian units): $\vec{\nabla}\times\vec{E}(\vec{x},t)=-(1/c)(\partial/\partial t)\vec{B}(\vec{x},t)$, $\vec{\nabla}\times\vec{H}(\vec{x},t)=(1/c)(\partial/\partial t)\vec{D}(\vec{x},t)$. Next we Fourier transform these equations to obtain

$$\vec{K}\times\vec{E}(\vec{K},\omega)=-\frac{\omega}{c}\vec{B}(\vec{K},\omega), \tag{A1}$$

$$\vec{K}\times\vec{H}(\vec{K},\omega)=\frac{\omega}{c}\vec{D}(\vec{K},\omega). \tag{A2}$$

We used the notation

$$\vec{E}(\vec{x},t)=\frac{1}{(2\pi)^4}\int_{-\infty}^{+\infty}d^3K d\omega\vec{E}(\vec{K},\omega)\exp[i(\vec{K}\cdot\vec{x}-\omega t)]. \tag{A3}$$

Multiplying Eq. (A1) by $\vec{K}\times$ from the left, substituting for $\vec{B}$ using the constitutive relation

$$\vec{B}(\vec{K},\omega)=\mu(\vec{K},\omega)\vec{H}(\vec{K},\omega), \tag{A4}$$

and substituting Eq. (A1) into the resulting equation, we obtain

$$\vec{K}\times\vec{K}\times\vec{E}(\vec{K},\omega)=-\frac{\mu\omega^2}{c^2}\vec{D}(\vec{K},\omega). \tag{A5}$$

We can write the constitutive equation relating the displacement and electric vectors as

$$\vec{D}(\vec{K},\omega)=\varepsilon(\vec{K},\omega)\vec{E}(\vec{K},\omega)+4\pi\vec{P}^{\rm nl}(\vec{K},\omega). \tag{A6}$$

The linear part of the polarization is given by $\vec{P}^L(\vec{K},\omega)=\chi^{(1)}(\vec{K},\omega)\vec{E}(\vec{K},\omega)$ where $\chi^{(1)}(\vec{K},\omega)=(4\pi)^{-1}[\varepsilon(\vec{K},\omega)-1]=(4\pi)^{-1}(n^2/\mu-1)$. In an isotropic homogeneous dispersive medium, the dielectric tensor ε is of the form of a dielectric constant times the unit tensor and the nonlinear polarization has components only in the direction of electric field $\vec{E}$, and $\vec{E}\perp\vec{K}$. Upon substituting Eq. (A5) into Eq. (A6) we obtain the dispersion relation

$$\left\{K^2-\frac{\omega^2}{c^2}n^2\right\}\vec{E}(\vec{K},\omega)=\frac{4\pi\omega^2}{c^2}\vec{P}^{\rm nl}(\vec{K},\omega). \tag{A7}$$

In deriving Eq. (A7) we used the identity $\vec{K}\times\vec{K}\times\vec{E}=\vec{K}(\vec{K}\cdot\vec{E})-K^2\vec{E}$. Equation (A7) determines $\vec{K}$ as a function of frequency ω, and the magnitude of the electric field (in an anisotropic medium, it is also a function of the direction propagation $\vec{s}$). If the nonlinear term is negligible, this equation yields the linear wave vector K^L, which is independent of the electric field amplitude, $K^L=n(\omega)\omega/c$. When the nonlinear term on the right hand side of Eq. (A7) is not entirely negligible, but still small, a perturbative approach can be used.

The nonlinear polarization appearing in Eq. (A6) can be approximated by the first few terms in the series expansion in powers of electric field. In glasses, crystals, and many other condensed phase media this series expansion converges for incident field strengths well below the optical damage threshold of the media. In many cases the first nonvanishing term is sufficient. For optical materials with a center of inversion symmetry, only odd powers appear in the expansion of the polarization in powers of the electric field strength E: $P^{\rm nl}=P^{\rm nl(3)}+P^{\rm nl(5)}+\cdots$. Expanding the wave vector on the left hand side of Eq. (A7) as $K=K^L+\delta K^{NL(2)}+\delta k^{NL(4)}+\cdots$ and substituting the expansion of the polarization into Eq. (A7) we find the following set of relations by comparing terms of the same order:

$$2K^L\delta K^{\rm nl(2)}\vec{E}(\vec{K},\omega)=\frac{4\pi\omega^2}{c^2}\vec{P}^{\rm nl(3)}(\vec{K},\omega), \tag{A8}$$

$$[2K^L\delta K^{\rm nl(4)}+(\delta K^{\rm nl(2)})^2]\vec{E}(\vec{K},\omega)=\frac{4\pi\omega^2}{c^2}\vec{P}^{\rm nl(5)}(\vec{K},\omega), \tag{A9}$$

etc. Note that in an isotropic medium, since the nonlinear polarization has the same direction as the driving electric field, $\delta K^{\rm nL}$ is along K^L.

2. First-order optical susceptibility: The linear term

If the amplitude of the electric field is small, we can neglect the influence of the nonlinear polarization. In this case the right hand side of the dispersion relation in Eq. (A7) is equal to zero. The slowly varying envelope of the electric field is defined by extracting the central K vector $\vec{K}_0$ and central frequency ω_0 of the pulse, $\vec{E}(\vec{x},t)=\vec{A}(\vec{x},t)\exp(i\vec{K}_0\cdot\vec{x}-\omega_0 t)$. It can be expanded in plane waves as

$$\vec{A}(\vec{x},t)=\frac{1}{(2\pi)^4}\int_{-\infty}^{+\infty}d^3K d\omega\ \vec{A}(\vec{K},\omega)\times\exp(i[\vec{K}-\vec{K}_0]\cdot\vec{x}-[\omega-\omega_0]t). \tag{A10}$$

To derive the propagation equation for the slowly varying envelope of the electric field we take the derivative of $\vec{A}(\vec{x},t)$ in the direction of the $\vec{s}_0=\vec{K}_0/|K_0|$, which we have chosen to be along the z axis:

$$\frac{\partial\vec{A}(\vec{x},t)}{\partial z}=\frac{1}{(2\pi)^4}\int_{-\infty}^{+\infty}d^3K d\omega\ (i[\vec{K}-\vec{K}_0]\cdot\vec{s}_0)\ \vec{A}(\vec{K},\omega)\times\exp(i[\vec{K}-\vec{K}_0]\cdot\vec{x}-[\omega-\omega_0]t). \tag{A11}$$

We may now substitute $[\vec{K}-\vec{K}_0]\cdot\vec{s}_0$ with K_z-K_0. Moreover, due to the dispersion relation quantities K_x, K_y, K_z,

and ω are not independent. It is consistent with our choice of propagation axis along z to relate K_z to the rest of the Fourier variables, $K_z - K_0 = f(K_x, K_y, \omega)$. We can now treat K_x, K_y, and ω as independent variables. It follows from Eq. (A10) that $\vec{A}(\vec{K},\omega)$ should be written as $\vec{A}(K_x,K_y,\omega)\,\delta(K_z - f(K_x,K_y,\omega))$. The integral over K_z in Eq. (A11) can be evaluated to obtain

$$\frac{\partial \vec{A}(\vec{x},t)}{\partial z} = \frac{1}{(2\pi)^4}\int_{-\infty}^{+\infty} dK_x dK_y d\omega\ \{i[f(K_x,K_y,\omega)]\} \times \vec{A}(K_x,K_y,\omega,z)\ \exp(i[K_x x + K_y y] - [\omega - \omega_0]t), \tag{A12}$$

where $\vec{A}(K_x,K_y,\omega,z) = \vec{A}(K_x,K_y,\omega)\ \exp\{i[f(K_x,K_y,\omega)]z\}$. Consequently we obtain the following differential equation in Fourier space for $\vec{A}(K_x,K_y,\omega,z)$:

$$\frac{\partial \vec{A}(K_x,K_y,\omega,z)}{\partial z} = \{i[f(K_x,K_y,\omega)]\}\vec{A}(K_x,K_y,\omega,z), \tag{A13}$$

whose solution is $\vec{A}(K_x,K_y,\omega,z) = \exp\{i[f(K_x,K_y,\omega)]z\}\,\vec{A}(K_x,K_y,\omega,0)$. Upon taking the inverse Fourier transform we obtain the solution for the pulse shape at any position z in real space.

3. Third-order optical susceptibility and the pulse propagation equation

Here we develop only with the lowest-order (third-order) nonlinear optical effects related to $P^{\mathrm{nl}(3)}$. In the Fourier domain, the nonlinear polarization $P^{\mathrm{nl}(3)}$ can be expanded as follows:

$$P_i^{\mathrm{nl}}(\vec{K},\omega) = \int_{-\infty}^{+\infty} d^3\vec{K}_1 d\omega_1 d^3\vec{K}_2 d\omega_2 d^3\vec{K}_3 d\omega_3 \chi^{(3)}_{i,j,k,l} \times(-\omega,-\vec{K};\omega_1,\vec{K}_1;-\omega_2,-\vec{K}_2;\omega_3,\vec{K}_3) \times \delta(\vec{K}-\vec{K}_1+\vec{K}_2-\vec{K}_3)\,\delta(\omega-\omega_1-\omega_2+\omega_3) A_j(\vec{K}_1,\omega_1)A_k^*(\vec{K}_2,\omega_2)A_l(\vec{K}_3,\omega_3). \tag{A14}$$

The expression for the nonlinear polarization in Eq. (A14) incorporates energy conservation and phase matching conditions. To third order, only the lowest-order nonlinear wave-vector component is necessary in the expansion of Eq. (A7), hence the equation for the nonlinear wave vector is given by

$$\delta K^{\mathrm{nl}}\vec{E}(\vec{K},\omega) = \frac{2\pi\omega}{nc}\vec{P}^{\mathrm{nl}}(\vec{K},\omega). \tag{A15}$$

To obtain an equation of motion for the SVE we expand the term $(i[\vec{K}-\vec{K}_0]\cdot\vec{s}_0) = (i[\{\vec{K}^L - \vec{K}_0^L\} + \vec{\delta}K^{\mathrm{nl}}]\cdot\vec{s}_0)$ around central wave vector K_0. The part of this expression which is enclosed in the curly brackets describes the linear response of the medium. The relation between K_x^L, K_y^L, K_z^L, and ω is given by the linear dispersion relation. Note that in an isotropic medium there is no difference between the definitions of linear and nonlinear K_x and K_y; the nonlinearity in our approach modifies only K_z. Following Eq. (A11) we divide the propagation equation into linear and nonlinear parts:

$$\frac{\partial \vec{A}}{\partial z} = \mathcal{O}^L\vec{A} + \mathcal{O}^{\mathrm{nl}}\vec{A}. \tag{A16}$$

$\mathcal{O}^L\vec{A}$ is the contribution associated with $\{\vec{K}^L - \vec{K}_0^L\}$ and $\mathcal{O}^{\mathrm{nl}}\vec{A}$ with the nonlinear term $\vec{\delta K}^{\mathrm{nl}}$. The linear part of Eq. (A16) can either be expanded to obtain a differential equation, or treated in the Fourier domain if we want to avoid the slowly varying envelope approximation and the paraxial approximation. To handle the nonlinear part, represented by $\vec{\delta K}^{\mathrm{nl}}$, we have to combine definitions (A8) and (A14). It is convenient to collect all factors depending on ω and $\vec{K}$ and combine then into a new function ψ:

$$\psi(-\omega,-\vec{K};\omega_1,\vec{K}_1;-\omega_2,-\vec{K}_2;\omega_3,\vec{K}_3) = \frac{2\pi\omega}{nc}\chi^{(3)}(-\omega,-\vec{K};\omega_1,\vec{K}_1;-\omega_2,-\vec{K}_2;\omega_3,\vec{K}_3). \tag{A17}$$

We introduce the abbreviated notation

$$\psi_{i,j,k,l}(-\omega_0,-\vec{K}_0;\omega_0,\vec{K}_0;-\omega_0,-\vec{K}_0;\omega_0,\vec{K}_0) = \psi_{i,j,k,l},$$

$$\frac{\partial}{\partial\omega_r}\psi_{i,j,k,l}(-\omega,-\vec{K};\omega_1,\vec{K}_1;-\omega_2,-\vec{K}_2;\omega_3,\vec{K}_3)\big|_{\omega=\omega_1=\omega_2=\omega_3=\omega_0} = \psi^r_{i,j,k,l},$$

where the superscript r indicates differentiation with respect to $r=0,\ldots,3$ the rth argument of $\psi_{i,j,k,l}$.

Using definitions (A10) and (A11), and expanding the ψ functions in all arguments around $(\omega_0,\vec{K}_0)$ we can perturbatively treat the nonlinear term:

$$\mathcal{O}^{\mathrm{nl}}A_i = \int_{-\infty}^{+\infty} d^3\vec{K}d\omega d^3\vec{K}_1 d\omega_1 d^3\vec{K}_2 d\omega_2 d^3\vec{K}_3 d\omega_3 A_j(\vec{K}_1,\omega_1)A_k^*(\vec{K}_2,\omega_2)A_l(\vec{K}_3,\omega_3)[\psi_{i,j,k,l} + (\omega-\omega_0)\psi^0_{i,j,k,l} + (\omega_1-\omega_0)\psi^1_{i,j,k,l} + (\omega_2-\omega_0)\psi^2_{i,j,k,l} + (\omega_3-\omega_0)\psi^3_{i,j,k,l} + \cdots]\delta(\vec{K}-\vec{K}_1+\vec{K}_2-\vec{K}_3)\,\delta(\omega-\omega_1+\omega_2-\omega_3)\exp(i[\vec{K}-\vec{K}_0]\cdot\vec{x} - [\omega-\omega_0]t) \tag{A18}$$

and apply the convolution theorem to obtain the propagation equation for the SVE in closed form. Pulse propagation is driven by a polarization given by a superposition of linear and third-order polarization terms:

$$\frac{\partial A_i}{\partial z}=\mathcal{O}_{ij}^{L}A_j+\psi_{i,j,k,l}A_jA_k^*A_l+\psi_{i,j,k,l}^0\frac{\partial(A_jA_k^*A_l)}{\partial t}+\psi_{i,j,k,l}^1\frac{\partial(A_j)}{\partial t}A_k^*A_l+\psi_{i,j,k,l}^2A_j\frac{\partial(A_k^*)}{\partial t}A_l+\psi_{i,j,k,l}^3A_jA_k^*\frac{\partial(A_l)}{\partial t}. \tag{A19}$$

In this presentation we treat the case of linearly polarized pulses. Hence, only two independent $\chi^{(3)}$ elements ($\chi_{xxzz}=\chi_1$ and $\chi_{xzzx}=\chi_2$) are present. The first nonlinear term is equal to $2\psi_1|A|^2A_i+\psi_2A^2A_i^*$, which for a linearly polarized pulse is simply $(2\psi_1+\psi_2)|A|^2A_i$. Terms including derivatives of ψ are related to the derivatives of χ^3 with respect to frequency. For example, the third term in Eq. (A19) is equal to

$$\psi_{i,j,k,l}^0=\frac{\partial}{\partial\omega}[2\pi\omega(nc)^{-1}\chi_{i,j,k,l}^{(3)}(-\omega,-\vec{K};\omega_1,\vec{K}_1;-\omega_2,-\vec{K}_2;\omega_3,\vec{K}_3)]=(\omega)^{-1}\psi_{i,j,k,l}+2\omega\pi(c)^{-1}\frac{\partial}{\partial\omega}$$
$$\times[n^{-1}\chi_{i,j,k,l}^{(3)}(-\omega,-\vec{K};\omega_1,\vec{K}_1;-\omega_2,-\vec{K}_2;\omega_3,\vec{K}_3)]. \tag{A20}$$

In our numerical examples we used short (femtosecond) pulses. Assuming that $\chi^{(3)}$ does not have resonances near the central frequency ω_0, we estimate that the contribution of the shock term should be of order $(\omega_0\tau_0)^{-1}$ times smaller than the contribution from the first nonlinear term in Eq. (A19). We checked the influence of the shock term on the dynamics and found that, in all but the anomalous dispersion regime where part of the pulse becomes extremely narrow in time, the contribution is negligible for the parameters employed over the propagation distances used in our presentation.

[1] J. E. Rothenberg, Opt. Lett. **17**, 583 (1992); **17**, 1340 (1992).

[2] P. Chernev and V. Petrov, Opt. Lett. **17**, 172 (1992).

[3] P. B. Corkum, C. Rolland, and T. Srinivasan-Rao, Phys. Rev. Lett. **57**, 2268 (1986); P. B. Corkum and C. Rolland, IEEE J. Quantum Electron. **25**, 2634 (1989).

[4] J. K. Ranka, R. W. Schirmer, and A. L. Gaeta, Phys. Rev. Lett. **77**, 3783 (1996).

[5] G. G. Luther, A. C. Newell, J. V. Moloney, and E. M. Wright, Opt. Lett. **19**, 789 (1994); **19**, 862 (1994).

[6] G. Fibich, Phys. Rev. Lett. **76**, 4356 (1996).

[7] L. Berge *et al.*, J. Opt. Soc. Am. B **13**, 1879 (1996).

[8] M. Trippenbach, T. C. Scott, and Y. B. Band, Opt. Lett. **22**, 579 (1997); T. C. Scott, M. Trippenbach, and Y. B. Band, Maple Tech. **4**(2), 63 (1997).

[9] Y. B. Band and M. Trippenbach, Phys. Rev. Lett. **76**, 1457 (1996).

[10] M. Trippenbach and Y. B. Band, J. Opt. Soc. Am. B **13**, 1403 (1996): C. Radzewicz, J. S. Krasinski, M. J. la Grone, M. Trippenbach, and Y. B. Band, *ibid.* **14**, 420 (1997).

[11] We carried out 3D calculations with cylindrical symmetry about the *z* axis and verified that the scenarios reported here also occur in the 3D case. M. Trippenbach and Y. B. Band (unpublished).

[12] B. C. Stuart, M. D. Feit, A. M. Rubenchik, B. W. Shore, and M. D. Perry, Phys. Rev. Lett. **74**, 2248 (1995).

[13] G. P. Agrawal, *Nonlinear Fiber Optics* (Academic Press, New York, 1989); M. Gedalin, T. C. Scott, and Y. B. Band, Phys. Rev. Lett. **78**, 448 (1997).